Experimental and Theoretical Study of Hall Field Limitations in MHD Generators

Wahid Hermina* and Charles H. Kruger†
Stanford University, Stanford, California

Experimental and theoretical results pertaining to the Hall field behavior in combustion-driven MHD generators using clean fuel are presented. MHD generators are subject to Hall field breakdown as a result of electrical-thermal instabilities within the interelectrode plasma region and the interelectrode insulator. Interelectrode breakdown within the insulator typically occurs at a lower threshold voltage than breakdown of the plasma itself. As a result, experiments have been carried out to study the effect on the insulator initiated breakdown threshold of interelectrode insulator cooling. Experiments have also been carried out to study the dependence of the breakdown threshold on the electrode boundary-layer Joule heating, insulator width, and magnetic field. A two-dimensional computer model of the plasma and insulator regions has been developed. Theoretical results based on this model are compared with experimental data. The comparisons indicate both qualitative and quantitative agreement between experiment and theory.

I. Introduction

ONE of the important problem areas of magnetohydrodynamic (MHD) power generation is the prevention of Hall field breakdown. As a result of large induced axial electric fields within the generator, electrical breakdown occurs between adjacent electrodes on the electrode walls. Unkel[1] has observed that the electrical breakdown arises from a thermal-electrical instability and that the breakdown can initiate either within the interlectrode insulator or the interelectrode plasma region. Several experimenters[1-5] have studied the dependence of the Hall field behavior on generator parameters such as electrode current density, magnetic field, insulator width, and electrode temperature.

This paper deals with both an experimental and theoretical study of the Hall field behavior in clean fuel combustion-driven MHD generators. The experimental objectives are twofold: to study the effects of various insulator cooling techniques on the insulator initiated breakdown threshold, and to study the dependence of the Hall field behavior on generator parameters such as insulator size, electrode boundary-layer Joule heating, and magnetic field. The experiments were performed in the Stanford M-2 facility. The flow train includes a combustor, plenum, test section, and diffuser. The reactants consist of ethanol seeded with potassium hydroxide, oxygen, and nitrogen diluent. Typical dimensions and other generator parameters can be found in Tables 1 and 2.

A two-dimensional coupled plasma-insulator model[6] was developed to study the dependence of the Hall field behavior on several generator design criteria. Results obtained with the model are compared to experimental data. The comparisons are favorable and identify several mechanisms occurring within the generator which significantly affect the Hall field behavior.

Received May 27, 1982; revision received Feb. 7, 1983.

*Presently member of Technical Staff, Thermal Sciences Division, Sandia Laboratories, Livermore, California.

†Professor, Department of Mechanical Engineering. Member AIAA.

II. Cooled Insulator Experiments

To sustain higher axial core fields, it is necessary to raise the voltage threshold for insulator thermal-electrical instability. This can be achieved by cooling the insulator. Three experiments have been performed under clean fuel and applied axial field conditions for the purpose of testing three insulator cooling techniques. The cooling techniques tested are internal cooling, film cooling, and insulator surface recession. The run conditions for each of the three experiments are listed in Table 1. The core velocities, core temperatures, and core electrical conductivities in this table are based on calculations with a one-dimensional plasmadynamic code for a location within the active region of the generator. In each of the experiments, all of the cooled insulators were compared with a reference solid magnorite insulator. In experiments 1 and 2, insulator widths ranged from 7.5 to 8.9 mm. In the third experiment, all the insulators were approximately 7.5-mm wide.

In all of the experiments, the upstream electrode of the axial pair was the cathode. Each electrode consisted of a stainless steel cap brazed to a water cooled copper base. Experimental operating conditions were chosen to ensure electrode surface temperatures of approximately 1100 K at zero electrical current. As a result, small differences in operating conditions existed among the experiments, as indicated by Table 1.

Table 1 Run condition for cooled insulator experiments

	Experiment 1	Experiment 2	Experiment 3
Mass flow rate, kg/s	0.136	0.113	0.113
Core velocity, m/s	360	300	300
Core temperature, K	2710	2690	2690
Core pressure, atm	1	1	1
N_2/O_2 ratio	0.5	0.5	0.5
Core electrical Conductivity, mho/m	10	9	9
Fuel	Ethanol	Ethanol	Ethanol
Stoichiometry	1.0	1.0	1.0
Channel height, cm	10	10	10
Channel width, cm	3	3	3
Electrode length, cm	1.9	1.9	1.9
Insulator length, cm	0.8	0.8	0.8
Potassium by weight, %	1	1	1

Table 2 Experimental run conditions and channel dimensions for applied and induced field experiments

Mass flow rate	0.17 kg/s
Core velocity	450 m/s
Core temperature	2750 K
Fuel	Ethanol
Stoichiometry	1.0
Core Hall parameter	0-1
Core pressure	1 atm
Core electrical conductivity	10 mho/m
Magnetic field	2.4 T
N_2/O_2 ratio	0.4
Potassium by weight	1.2%
Channel height (insulator wall)	10 cm
Channel width (electrode wall)	3 cm
Electrode pitch	3.8 cm
Distance from nozzle	33-60 cm

A. Insulator Designs

Normal Magnorite Insulators

The normal test insulators were constructed from magnorite, a magnesium oxide (Mg0) based ceramic produced by the Norton Corporation. The insulators were mounted between adjacent electrodes so as to be flush with the electrode surfaces. RTV silicone rubber was used to bond the insulator underside to the cooled electrode wall. Thermal contact also arises between the insulator and adjacent electrodes during the experiment as a result of thermal expansion of the electrode wall components. The predominant cooling mechanisms for this insulator design are surface radiation and thermal conduction to the adjacent electrodes and cooled wall.

Internally Cooled Insulators

Two internally cooled insulator designs were tested. In the second experiment, a 3.2-mm thick, 85%-dense Mg0 rectangular slab was bonded to a water cooled metal section. The bonding agent was a thin layer of RTV silicone rubber. In addition to the water cooling from below, the electrode edges adjacent to the insulator were cooled by nitrogen gas to provide cooling for the insulator. The 85%-dense Mg0 is more densely packed and has a smaller grain size than the magnorite.

In the third experiment, a boron nitride (BN) insulator was tested. The BN insulator was bonded to a water cooled copper section. The bonding agent was a copper based ceramic adhesive. The intended design point for the BN insulator was a surface temperature of 1100 K, however, as a result of surface spalling due to trapped water vapor, the thermal conductance path for insulator cooling was disrupted, thereby giving rise to surface hot spots and consequent melting of the insulator surface.

Film Cooled Insulators

Film cooling was tested in experiments 1 and 3. In both cases, a slot was machined into the downstream edge of the electrode, just upstream of the insulator. The slot ran the entire width of the MHD channel. Nitrogen gas was injected into the boundary layer through the slot. In the first experiment, the slot thickness was 0.20 mm and the coolant flow rate was 0.35 g/s; in the third expeirment, the slot width was increased to 0.80 mm and the coolant flow rate was maintained at 0.35 g/s. The performance of the 0.80-mm slot was superior to that of the 0.20-mm slot because of substantially reduced blockage of the slot exit by condensation from the plasma.

Recessed Insulators

Two magnorite insulators were tested with different surface recession depths. In the second experiment a magnorite insulator was recessed 6 mm relative to the adjacent electrode surface. In the third experiment, the recession depth was reduced to 2 mm. It was found that in both cases the recession induced large-scale fluctuations in the electrical behavior. Although surface recession did prevent insulator initiated breakdown, it apparently enhanced plasma initiated breakdown.

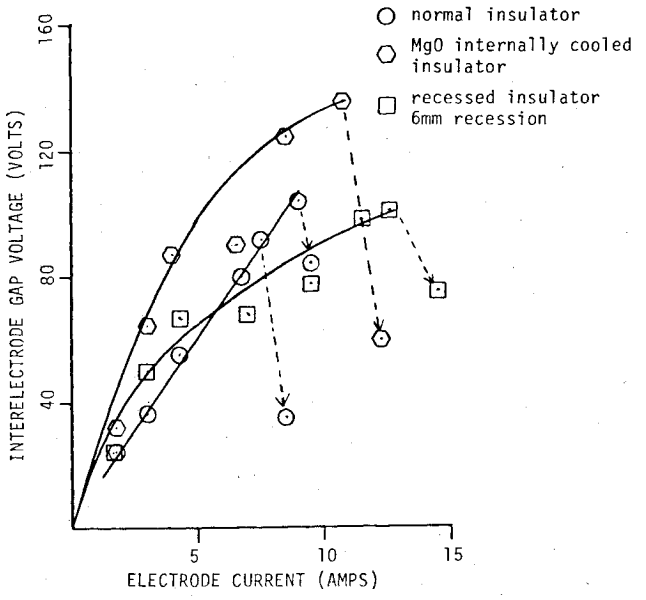

Fig. 1 Interelectrode gap voltage vs electrode current; data from experiment 2.

B. Experimental Results

Figures 1 and 2 contain experimental results for the various cooled insulator designs and the normal insulator tested in experiments 2 and 3. Figure 1 indicates that the Mg0 internally cooled insulator sustained a gap voltage of 135 V prior to breakdown as compared to 105 V for the normal test insulator. The breakdown mode for the cooled insulator was internal, occurring between the electrodes and the insulator metal cooling section. The recessed insulator sustained a breakdown threshold of 101 V, comparable to that of the normal test insulator.

Figure 2 indicates that the film cooled insulator sustained a breakdown threshold of 118 V as compared to 93 V for the normal test insulator. The breakdown mode for the film cooled insulator was plasma initiated. The BN insulator sustained an initial breakdown threshold of 110 V. However, subsequent breakdowns occurred at lower voltages due to degradation of the insulator. BN is hygroscopic; as a result, the surface is subject to surface spalling at high temperatures due to the vaporization of the trapped water. This degrades the cooling of the surface and thereby reduces the breakdown threshold. Long duration tests[7] indicate that 0.191-cm-thick BN insulators inserted between copper electrodes can survive several hundred hours of operation. However, despite the improved cooling and lower insulator surface temperatures, insulator surface recession still was observed.

The recessed insulator results of Fig. 2 indicate a breakdown threshold of 95 V, comparable to that of the normal test insulator. The overall performance of the recessed insulators described in both Figs. 1 and 2 was inferior to that of the normal test insulators. Seed products would condense in the recession, shorting out the gap and, consequently, vaporizing as a result of the internal Joule heating within the deposit. The resulting gap voltage time history was unsteady.

III. Applied and Induced Field Experiments

Two experiments have been run with the complete Stanford M-2 channel to study the dependence of the interelectrode

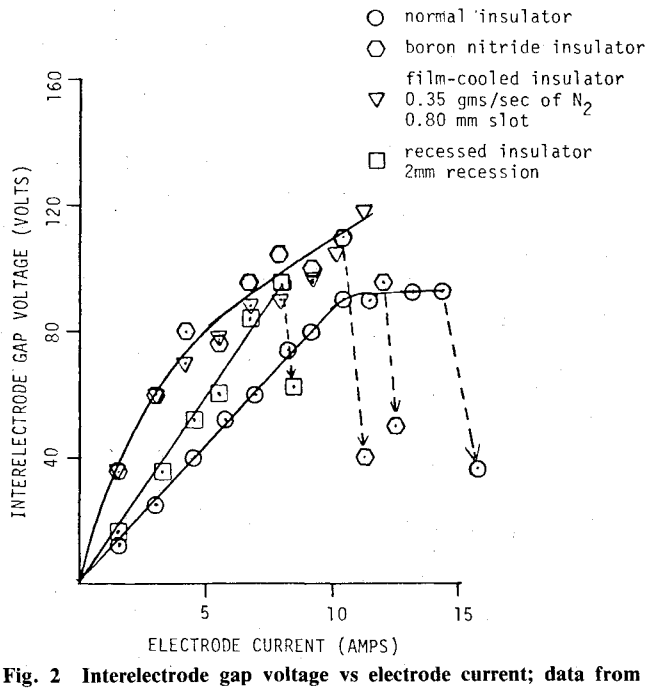

Fig. 2 Interelectrode gap voltage vs electrode current; data from experiment 3.

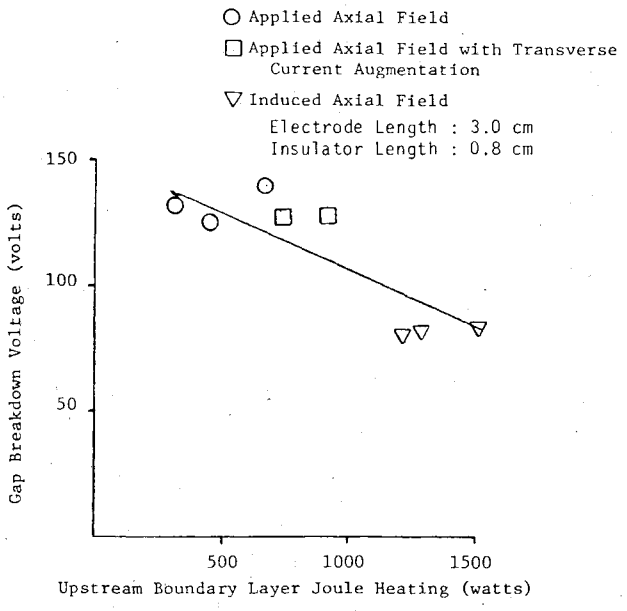

Fig. 3 Interelectrode gap breakdown voltage vs upstream electrode boundary-layer Joule heating for 0.8-cm insulators.

breakdown threshold on generator parameters such as the electrode boundary-layer Joule heating, insulator width, and magnetic field. To permit independent variation of the various generator parameters, four external electrical configurations were employed[6]: applied axial field between two adjacent electrodes, applied axial field with transverse current augmentation at the upstream electrode pair, applied axial field with transverse current augmentation at both the upstream and downstream electrode pairs, and induced axial field.

Three insulator sizes were tested: 0.2, 0.4, and 0.8 cm. The insulators were made from magnorite, a MgO based ceramic, and were mounted in the electrode walls such that the insulator surfaces were flush with the surfaces of the adjacent electrodes. Several insulators of each size were tested so as to permit observations of the electrical breakdowns for each of the electrical configurations. The electrodes were made from stainless steel and were designed to operate at approximately 1100 K surface temperature at zero current. The electrode lengths were adjusted so as to maintain a constant 3.8-cm pitch. Iridum voltage pins were inserted through the channel sidewall adjacent to the electrode surfaces to permit measurement of the boundary-layer voltage drops.

The experiments were performed under clean fuel conditions. The run conditions and generator dimensions for both experiments are listed in Table 2.

A. Experimental Results

Table 3 contains breakdown time constants for each experimental run series. Based on these time constants, the breakdown mode can be deduced. Typical time constants for insulator initiated breakdown are of the order of 100 ms while typical time constants for plasma initiated breakdown are of the order of 1 ms. Consequently, all of the 0.4- and 0.8-cm insulators experienced insulator initiated breakdown while the 0.2-cm insulator experienced plasma initiated breakdown.

Figure 3 contains experimental results for gap breakdown voltage vs upstream boundary-layer Joule heating for the 0.8-cm insulators. The upstream boundary-layer Joule heating is calculated from the product of the boundary-layer voltage drop and electrode current at the electrode upstream of the test gap. The boundary-layer voltage drop for this calculation is obtained by adding the measured induced voltage between the voltage pin and electrode at zero current to the measured voltage between the voltage pin and electrode with current flow. The data indicate that an increase in the boundary-layer Joule heating reduces the sustainable gap voltage. This can be attributed in part to the increased insulator heat flux resulting from Joule heating originating in the upstream boundary layer and convected to the downstream insulator. It can also be attributed in part to a reduction in insulator cooling resulting from an increased electrode surface temperature brought about by increased electrode boundary-layer Joule heating. The lower breakdown thresholds for the induced field results also can be partly attributed to seed condensation. The induced field results for the 0.8-cm insulators were obtained a few days after the applied fields results. Seed condensate, therefore, had more time to penetrate the interlectrode insulators for the induced field case.

Figure 4 is a plot of the breakdown thresholds vs upstream electrode boundary-layer Joule heating for the 0.4-cm insulators. These data indicate a reduction in the breakdown threshold from 74 to 60 V as the upstream boundary-layer Joule heating increases from 220 to 1400 W. This behavior agrees with that of Fig. 3 and can be attributed to the increased insulator surface temperatures resulting from the electrode boundary-layer Joule heating. One can also observe from Fig. 4 that the induced field data fall between the two sets of applied field data. This adds credence to the postulate that differences between applied field breakdown data and induced field breakdown data can be attributed to differences in the electrode boundary-layer Joule heating. The data in Fig. 4, unlike those of Fig. 3, were obtained in a single day, thereby minimizing the dependence of the breakdown threshold on seed condensation.

Figure 5 is a plot of the interelectrode gap breakdown voltage and breakdown electric field vs insulator width for the applied axial field data. One can observe that the sustainable gap voltage drops with decreasing insulator width, however, the sustainable gap axial electric field increases with a decrease in the insulator width. The latter effect can be attributed to thermal mechanisms. Two of these mechanisms are described. First, a reduction in the insulator width improves axial thermal conduction from the insulator to the cooler eletrodes; this reduces the insulator surface temperature and thereby reduces the internal Joule heating. Secondly, as a result of the boundary-layer thermal equilibration length, the colder boundary layer flowing from the

upstream electrode over the insulator becomes more significant in reducing surface heat flux as the insulator width is reduced. The reduced insulator surface heat flux leads to a reduction in the insulator surface temperature and a corresponding reduction in the internal Joule heating. Both of these mechanisms are deduced from theoretical results. Comparison of the data for the 0.2-cm insulator with those of the 0.4- and 0.8-cm insulators indicates that as the insulator size is reduced, and the corresponding thermal loading of the insulator is reduced, the breakdown mode changes from insulator initiated to plasma initiated.

Figure 6 contains experimental data of gap breakdown voltage and breakdown electric field as a function of insulator width for the induced axial field cases. As described previously for the applied axial field data, a reduction in insulator width reduces the gap breakdown voltage but increases the gap breakdown electric field. The explanations for the latter effect are the same as those described previously.

A consequence of the results plotted in both Fig. 5 and 6 is that for a given ratio of insulator size to electrode size, a reduction in the insulator width will increase the sustainable axial core fields. A technique for improving the Hall field performance of a generator, therefore, is to scale down the

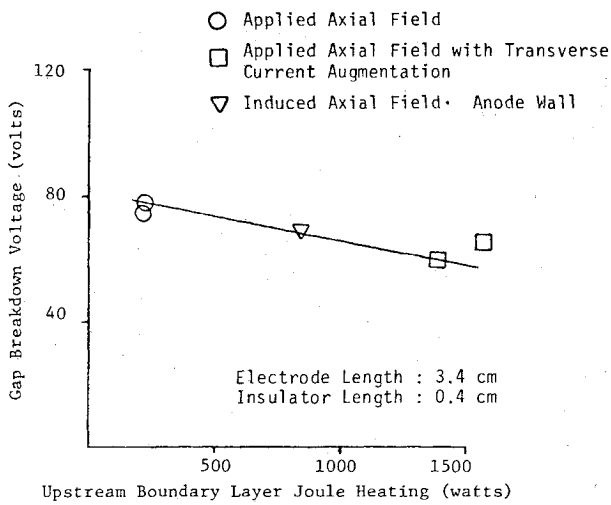

Fig. 4 Interelectrode gap breakdown voltage vs upstream electrode boundary-layer Joule heating for 0.4-cm insulators.

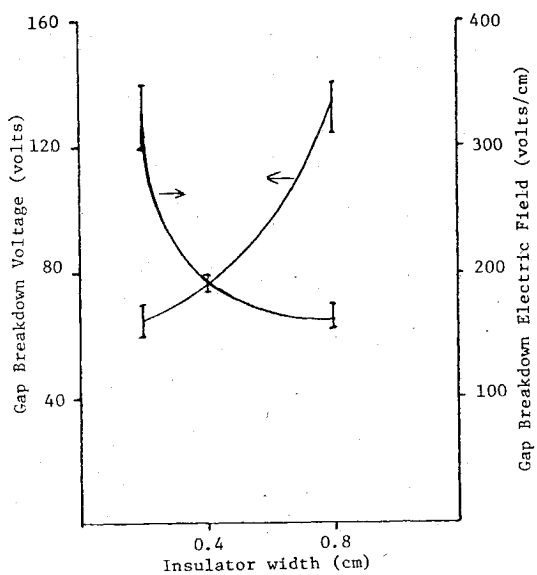

Fig. 5 Interelectrode gap breakdown voltage and electric field vs insulator width for applied axial field results; electrode pitch of 3.8 cm.

components on the electrode wall, maintaining, however, a fixed ratio of electrode to insulator width. Figures 5 and 6 also indicate that for a constant electrode pitch, increasing the insulator size raises the breakdown voltage threshold. This dependence of the breakdown voltage on insulator size is governed by the sensitivity of the insulator thermal loading to the insulator size. Other experimenters[2] have found a much weaker dependence of the breakdown voltage on insulator size indicating a more sensitive dependence of insulator thermal loading to insulator size for their configuration.

Figure 7 contains insulator surface temperature data measured by an optical pyrometer. The data were taken from applied field configurations with and without transverse current augmentation for a 0.8-cm insulator. One can observe that as the upstream current increases, the insulator surface temperature rises. This can be attributed in part to the electrode boundary-layer Joule heating which is convected to the downstream insulator; in part to the Joule heating induced increase of the electrode surface temperature which degrades the cooling of the adjacent insulators; and in part to increased Joule heating within the insulator. The data indicate that insulator initiated breakdown occurs at an insulator surface temperature of around 2100 K for MgO insulators. The data also indicate the presence of insulator hot spots just prior to insulator initiated breakdown. Figure 7 indicates a hot spot temperature of 2310 K at an electrode current of 12 A for the applied axial field case and a hot spot temperature of 2235 K at an electrode current of 25 A for the applied axial field case with transverse current augmentation. This agrees well with theoretical predictions that insulator initiated breakdown results from a thermal instability caused by internal Joule heating.

IV. Theoretical Model

A two-dimensional computer program has been developed to model the plasma and interelectrode insulator regions of an MHD generator.[6] The model is comprised of four parts: the plasma dynamic conservation equations, the electron dynamic equations, three plasma electrical models, and two interelectrode insulator thermal-electrical models.

The plasma dynamic conservation equations consist of the real gas compressible continuity, axial momentum, and energy equations in the boundary-layer approximation.[6,8,9] In addition, a model for the transverse pressure distribution is included.[6,9] The electron dynamic conservation equations consist of the electron continuity[6,8,9] and electron energy[6,10] equations.

Three plasma electrical models have been included for the purpose of calculating the local plasma current densities. A

Table 3 Breakdown time constants for applied and induced field experiments

Experiment	Time, ms
Applied field, 0.8-cm insulator,	30, 47 (insulator initiated)
Applied field with transverse augmentation, 0.8-cm insulator	180 (insulator initiated)
Applied field, anode wall 0.8-cm insulator	600 (insulator initiated)
Applied field, cathode wall 0.8-cm insulator	780 (insulator intiated)
Induced field, anode wall 0.8-cm insulator	1000 (insulator initiated)
Applied field, 0.4-cm insulator	130 (insulator initiated)
Applied field with transverse augmentation, 0.4-cm insulator	190 (insulator initiated)
Induced field, anode wall 0.4-cm insulator	690 (insulator initiated)
Applied field, 0.2-cm insulator	3 (plasma initiated)

finite element model developed by Oliver[6,9,11] provides the simplest approximation to the plasma currents. In addition, a current concentration model[6,10] has been developed which provides the computational speed of Oliver's electrical model and also permits computation of the current concentration on the electrode surface. The third plasma electrical model solves the two-dimensional intergral and differential forms of Maxwell's equations[6,10] for the current streamlines in the plasma. From the current streamlines the plasma current densities are calculated.

Two insulator thermal-electrical models have been incorporated in the program. A one-dimensional model[6,9] permits variations in axial current density and properties normal to the insulator-plasma interface. A quasi-two-dimensional model[6,9] permits property variations in two dimensions but only permits axial current density variations normal to the insulator-plasma interface. For both insulator models, the insulator transverse current density is neglected.

The program can be used to model the plama and insulator response to electrical loading of the generator. The program can also be used to predict the onset of both insulator and plasma initiated breakdown.

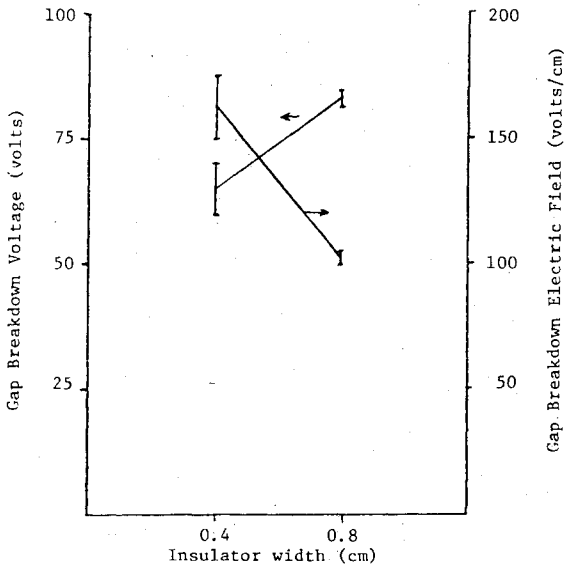

Fig. 6 Interelectrode gap breakdown voltage and electric field vs insulator width for induced axial field results; electrode pitch of 3.8 cm.

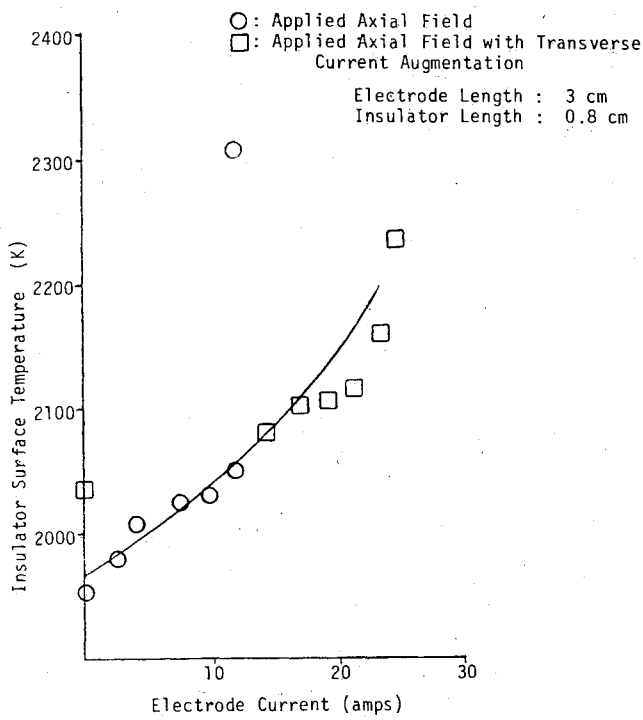

Fig. 7 Insulator surface temperature vs upstream electrode current for applied axial field results.

V. Comparison of Theoretical and Experimental Results

The theoretical model has been used to study the dependence of the Hall field breakdown threshold on several generator parameters.[6] In addition, theoretical results have been obtained that permit comparison with experimental data. In the following paragraphs theoretical results are compared with experimental data for gap voltage, plasma axial voltage, boundary-layer voltage drop, and electrode surface temperature elevation vs transverse current density. Comparisons are made for both 0.4- and 0.8-cm insulators. The generator conditions for the theoretical runs were chosen to match the experimental conditions listed in Table 2.

Figure 8 compares experimental data and theoretical results for gap voltage and plasma axial voltage vs core current density for 0.8-cm insulators. The results indicate good agreement between the measured plasma voltages and the theoretical results. The plasma voltages are measured between two adjacent pins positioned outside the boundary layer and near the leading edges of two adjacent electrodes. The measured gap voltage is larger than the calculated values as a result of unequal boundary-layer voltage drops in the experiments for the electrodes adjacent to the test gap. Both the theory and experiment indicate insulator initiated breakdown thresholds of around 80 V.

Figure 9 compares experimental and theoretical results for 0.4-cm insulators. As before, the measured plasma voltage

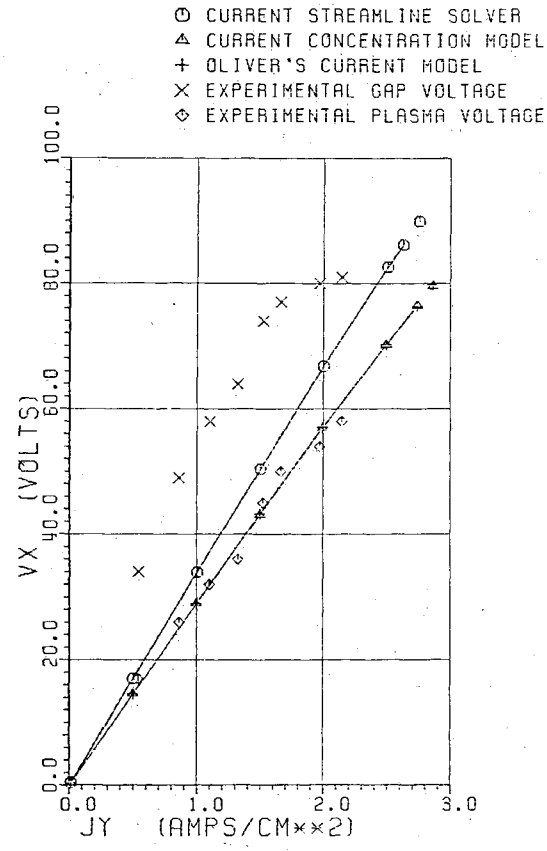

Fig. 8 Interelectrode gap voltage and plasma axial voltage vs core current density; comparison of experiment and theory for 0.8-cm insulators.

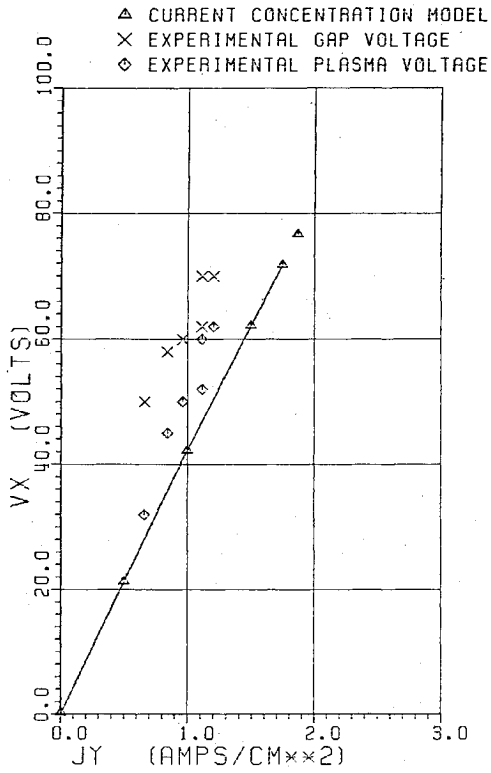

Fig. 9 Interelectrode gap voltage and plasma axial voltage vs core current density; comparison of experiment and theory for 0.4-cm insulators.

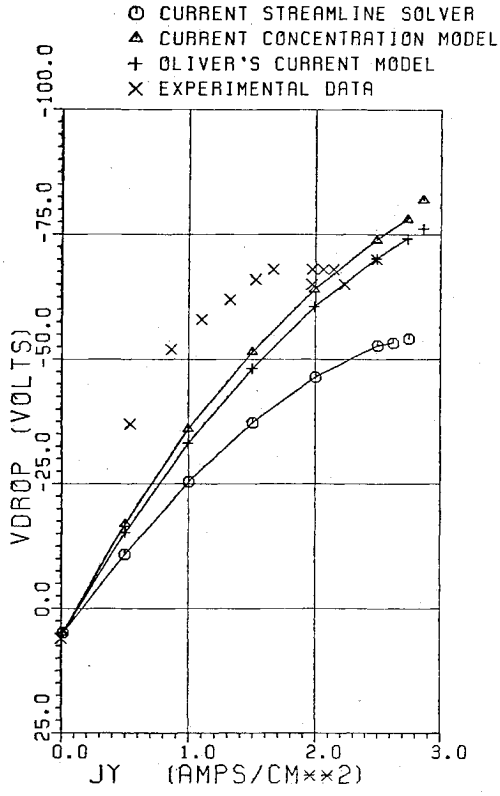

Fig. 10 Electrode voltage drop at 1.0 cm from leading edge vs core current density.

differences agree with the calculated gap voltages although the measured gap voltages are higher than the calculated values. Both the theoretical results and experimental data indicate insulator initiated breakdown at a gap voltage of around 70 V. The temperature-dependent function which was used to describe the insulator electrical conductivity for the

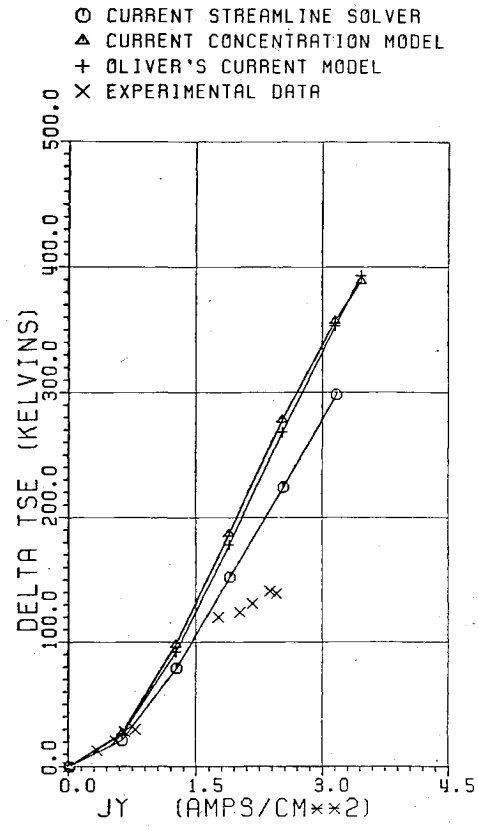

Fig. 11 Electrode surface temperature rise vs electrode current density.

theoretical results in Fig. 8 was multiplied by 1.4 for the theoretical results in Fig. 9. This 40% increase in insulator electrical conductivity for the 0.4-cm insulator is based on the experimental observation that reductions in the insulator surface temperature increase seed product condensation.[12] Based on theoretical results, the 0.4-cm insulator operates at a surface temperature 140 K below the 0.8-cm insulator. Therefore, it is expected that the insulator will suffer from higher levels of seed condensation and a corresponding reduction in electrical resistivity.

Figure 10 is a plot of the boundary-layer voltage drop vs core current density. The results indicate that the measured boundary-layer voltage drops are somewhat larger than those predicted by the theory. At the higher current levels the measured data agrees with the theoretical results obtained from the current concentration plasma model and Oliver's plasma model.[11] However, as a result of the intense current concentration at the electrode leading edge predicted by the current streamline solver, the predicted boundary-layer voltage drop at 1 cm from the leading edge is appreciably lower than the measured values. These results suggest that the presence of micro-arcing in the experiments may favor current streamlines different from those that are predicted by a diffuse current model.

Figure 11 is a plot of electrode surface temperature elevation vs core current density. The results indicate good agreement between experiment and theory, especially for the lower current densities. The differences between the theory and experiment for the higher currents can be attributed in part to the presence of micro-arcing in the experiments. Micro-arcing reduces the average Joule heating in the near-wall regions of the boundary layer, which in turn reduces the electrode surface temperature elevation.

V. Conclusions

Based on the experimental and theoretical results just presented several conclusions pertaining to Hall field

limitations can be drawn. The results indicate that insulator-initiated breakdown is brought about by an electrical-thermal instability within the insulator, resulting from Joule heating within the plasma boundary layer and insulator.

Increasing the Joule heating within the boundary layer upstream of the insulator reduces the insulator-initiated breakdown threshold as a result of the increased insulator thermal loading. The latter observation explains the observed differences in the breakdown threshold between applied and induced axial field results. For magnetic field strengths typical of those in the present experiments, the electrode currents and corresponding boundary-layer Joule heating required to induce a particular axial field are larger than those required under applied axial field conditions. The insulator-initiated breakdown thresholds, therefore, are lower under induced field conditions than under applied field conditions. The present results indicate that the primary dependence of the breakdown threshold on magnetic field results from the dependence of the boundary-layer Joule heating on magnetic field.

Comparison between the experimental and theoretical results have indicated the existence of two competing processes as the insulator surface temperature is reduced. Reductions of the surface temperature raise the electrical resistivity of the pure insulator; however, lower surface temperatures increase the seed condensation from the plasma into the insulator. For the magnorite insulators tested in the present experiments, the resulting effect is that reductions in the insulator surface temperatures lead to higher sustainable axial electric fields at the insulator surfaces. The present results indicate that, as a result of insulator cooling via conduction to the adjacent electrodes, the sustainable insulator and core axial electric fields can be increased by scaling down both the electrodes and insulators, while maintaining a constant ratio of insulator width to electrode pitch. The present experimental results also indicate that reductions in the insulator surface temperature will eventually raise the breakdown threshold to that of plasma-initiated breakdown.

References

[1]Unkel, W. and Kruger, C. H., "Axial Field Limitations in MHD Generators," 16th Symposium on Engineering Aspects of MHD, University of Pittsburgh, Pittsburgh, Penn., May 1977.

[2]Zalkind, V. I., Kirillov, V. V., Tikhotsky, A. S. and Vstenskaya, G. L., "Experimental Investigation of Interelectrode Breakdown in MHD Channels," 7th International Conference on MHD Electric Power Generation, MIT, Cambridge, Mass., June 1980.

[3]Bystriy, A. M. Ganefel'd, R. V., Mazur, N. I., Miroshnichenko, A. A., Naletov, V. V., Nekhamin, M. M. and Red'kin, V. B., "Investigation of Turbulence and Electric Discharge Processes in an MHD Channel," 7th International Conference on MHD Electric Power Generation, MIT, Cambridge, Mass. June 1980.

[4]Dubok, V. A., Mazur, N. I. and Miroshnichenko, A. A., "Prebreakdown Phenomena and Breakdown in the Magnesium Oxide Insulators in the Channel of an MHD Generator," 7th International Conference on MHD Electric Power Generation, MIT, Cambridge, MIT, Cambridge, Mass., June 1980.

[5]Unkel, W. C., "Axial Field Limitations in MHD Generators," Stanford University, Stanford, Calif., HTGL Rept. 107 and Ph.D. Thesis, April 1978.

[6]Hermina, W. L., "Hall Field Limitations in MHD Generators," Ph.D. Thesis, Stanford University, Stanford, Calif., April 1982.

[7]Demirjian, A. et al., "Long Duration Channel Development and Testing," 18th Symposium on Engineering Aspects of MHD, Butte, Montana, June 1979.

[8]James, R. K., "Joule Heating Effects in the Electrode Wall Boundary Layer of MHD Generators," HTGL Rept. 115 and Ph.D. Thesis, Stanford University, Stanford, Calif., Jan. 1980.

[9]Hermina, W. L. and Kruger, C. H., "Plasma and Insulator Initiated Hall Field Breakdown," 19th Symposium on the Engineering Aspects of MHD, UTSI, June 1981,

[10]Hermina, W. L. and Kruger, C. H., "Experimental and Theoretical Study of Hall Field Breakdown," 20th Symposium on the Engineering Aspects of MHD, University of California at Irvine, June 1982.

[11]Oliver, D. A., "The Prediction of Interelectrode Breakdown in Magneto-hydrodynamic Generators," 14th Symposium on Engineering Aspects of MHD, UTSI, Tullahoma, Tenn. April 1974.

[12]Furuse, Y., Amemiya, Y., Hayashi, Y., Kato, T., Fukui, T., Shiota, M., "Study on Refractory Materials for the MHD Electric Power Generation (Part 3) Electrical Behavior of Various Types of Mg0 Refractories," Research Laboratory Report, Asahi Glass Co., Japan, Vol. 20, 1970.

U.S. Postal Service

STATEMENT OF OWNERSHIP, MANAGEMENT AND CIRCULATION

Required by 39 U.S.C. 3685) ISSN # 0001-1452

1A. TITLE OF PUBLICATION	1B. PUBLICATION NO.	2. DATE OF FILING
AIAA JOURNAL	0 0 9 9 2 0	NOV. 8,1983

3. FREQUENCY OF ISSUE	3A. NO. OF ISSUES PUBLISHED ANNUALLY	3B. ANNUAL SUBSCRIPTION PRICE
MONTHLY	12	$19.00

4. COMPLETE MAILING ADDRESS OF KNOWN OFFICE OF PUBLICATION *(Street, City, County, State and ZIP Code) (Not printers)*

1633 BROADWAY, NEW YORK, N.Y. 10019

5. COMPLETE MAILING ADDRESS OF THE HEADQUARTERS OF GENERAL BUSINESS OFFICES OF THE PUBLISHER *(Not printer)*

SAME AS ABOVE

6. FULL NAMES AND COMPLETE MAILING ADDRESS OF PUBLISHER, EDITOR, AND MANAGING EDITOR *(This item MUST NOT be blank)*

PUBLISHER *(Name and Complete Mailing Address)*

AMERICAN INSTITUTE OF AERONAUTICS AND ASTRONAUTICS, INC. SAME AS ABOVE

EDITOR *(Name and Complete Mailing Address)*

GEORGE W. SUTTON SAME AS ABOVE

MANAGING EDITOR *(Name and Complete Mailing Address)*

ELAINE J. CAMHI SAME AS ABOVE

7. OWNER *(If owned by a corporation, its name and address must be stated and also immediately thereunder the names and addresses of stockholders owning or holding 1 percent or more of total amount of stock. If not owned by a corporation, the names and addresses of the individual owners must be given. If owned by a partnership or other unincorporated firm, its name and address, as well as that of each individual must be given. If the publication is published by a nonprofit organization, its name and address must be stated.) (Item must be completed.)*

FULL NAME	COMPLETE MAILING ADDRESS
AMERICAN INSTITUTE OF AERONAUTICS AND ASTRONAUTICS, INC.	SAME AS ABOVE

8. KNOWN BONDHOLDERS, MORTGAGEES, AND OTHER SECURITY HOLDERS OWNING OR HOLDING 1 PERCENT OR MORE OF TOTAL AMOUNT OF BONDS, MORTGAGES OR OTHER SECURITIES *(If there are none, so state)*

FULL NAME	COMPLETE MAILING ADDRESS
NONE	

9. FOR COMPLETION BY NONPROFIT ORGANIZATIONS AUTHORIZED TO MAIL AT SPECIAL RATES *(Section 423.12 DMM only)*
The purpose, function, and nonprofit status of this organization and the exempt status for Federal income tax purposes *(Check one)*

(1) [x] HAS NOT CHANGED DURING PRECEDING 12 MONTHS (2) [ ] HAS CHANGED DURING PRECEDING 12 MONTHS *(If changed, publisher must submit explanation of change with this statement.)*

10. EXTENT AND NATURE OF CIRCULATION	AVERAGE NO. COPIES EACH ISSUE DURING PRECEDING 12 MONTHS	ACTUAL NO. COPIES OF SINGLE ISSUE PUBLISHED NEAREST TO FILING DATE
A. TOTAL NO. COPIES *(Net Press Run)*	5,767	5,900
B. PAID CIRCULATION 1. Sales through dealers and carriers, street vendors and counter sales	-----	-----
2. Mail Subscription	5,048	5,213
C. TOTAL PAID CIRCULATION *(Sum of 10B1 and 10B2)*	5,048	5,213
D. FREE DISTRIBUTION BY MAIL, CARRIER OR OTHER MEANS SAMPLES, COMPLIMENTARY, AND OTHER FREE COPIES	74	73
E. TOTAL DISTRIBUTION *(Sum of C and D)*	5,122	5,286
F. COPIES NOT DISTRIBUTED 1. Office use, left over, unaccounted, spoiled after printing	645	614
2. Return from News Agents	-----	-----
G. TOTAL *(Sum of E, F1 and 2 - should equal net press run shown in A)*	5,767	5,900

11. I certify that the statements made by me above are correct and complete — SIGNATURE AND TITLE OF EDITOR, PUBLISHER, BUSINESS MANAGER, OR OWNER: CHRISTOPHER TROLE, ADMINISTRATOR, FINANCE & M.I.S